MATERIALS SCIENCE

Passive radiofrequency x-ray dosimeter tag based on flexible radiation-sensitive oxide field-effect transistor

Tobias Cramer[1]*, Ilaria Fratelli[1], Pedro Barquinha[2], Ana Santa[2], Cristina Fernandes[2], Franck D'Annunzio[3], Christophe Loussert[3], Rodrigo Martins[2], Elvira Fortunato[2], Beatrice Fraboni[1]

Distributed x-ray radiation dosimetry is crucial in diverse security areas with significant environmental and human impacts such as nuclear waste management, radiotherapy, or radioprotection devices. We present a fast, real-time dosimetry detection system based on flexible oxide thin-film transistors that show a quantitative shift in threshold voltage of up to 3.4 V/gray upon exposure to ionizing radiation. The transistors use indium-gallium-zinc-oxide as a semiconductor and a multilayer dielectric based on silicon oxide and tantalum oxide. Our measurements demonstrate that the threshold voltage shift is caused by the accumulation of positive ionization charge in the dielectric layer due to high-energy photon absorption in the high-*Z* dielectric. The high mobility combined with a steep subthreshold slope of the transistor allows for fast, reliable, and ultralow-power readout of the deposited radiation dose. The order-of-magnitude variation in transistor channel impedance upon exposure to radiation makes it possible to use a low-cost, passive radiofrequency identification sensor tag for its readout. In this way, we demonstrate a passive, programmable, wireless sensor that reports in real time the excess of critical radiation doses.

INTRODUCTION

Exposure to ionizing radiation has to be tightly controlled in radiotherapy, nuclear waste management, high-energy physics experiments, and space missions to avoid health or technical safety risks (*1*–*4*). Real-time information about radiation dose can be acquired by air ionization chambers or calorimetric detectors that provide accurate data for calibration but exhibit bulky cases and require complex control and readout electronics (*5*). In many applications, it is desired to have a distributed network of miniaturized, solid-state dosimeters that combine a compact, low-power electronic readout and a small and robust design to achieve a spatial map of the deposited dose. In medical scenarios, where radiation doses on human skin or in human organs have to be assessed, flexibility and high integration density of the sensor array are further crucial properties (*6*, *7*). Moreover, the possibility of wireless communication would allow the facile integration of a network of sensors over large areas to monitor or detect radiation contamination sources. To achieve such novel dosimeter applications, material sciences and electronic engineering have to develop new detector materials and electronic device architectures that combine high charge generation efficiency with the possibility to process them on flexible and large-area plastic substrates and high-bandwidth electronic operation and amplification for wireless integration (*8*, *9*).

To date, microelectronic dosimeters are realized in silicon-based complementary metal-oxide semiconductor (CMOS) technology and consist in diode or transistor structures (*10*). Upon exposure to ionizing radiation, defects are introduced or generated charge carriers get trapped in the active layers, causing a shift in device characteristics that is proportional to the absorbed radiation dose. Dosimetry in the dose ranging from a few hundreds of micro-grays up to several hundreds of grays, relevant for many dosimetry applications, is achieved in radiation-sensitive field-effect transistors (RADFET) that use a thick silicon oxide layer as a dielectric and a crystalline silicon channel (*11*–*13*). Upon exposure to radiation, excitons are generated in the dielectric and separate into hole and electron charge carriers that populate the valence and conduction bands of the dielectric (Fig. 1A). Electrons are mobile in the RADFET silicon oxide dielectric and hence diffuse out of the dielectric layer. Instead, hole charges get trapped and lead to the buildup of a positive ionization charge in the dielectric. The consequence is a shift in transistor threshold voltage toward negative values as the positive space charge in the dielectric contributes to the field effect in the semiconducting channel (*14*, *15*). The amount of threshold voltage shift is proportional to the total absorbed dose in the dielectric over a wide energy range and hence provides integrated information about the radiation exposure history (*7*, *16*). RADFET sensitivities are expressed as threshold voltage shift per radiation dose and amount to typical values of 0.05 to 0.3 V/Gy for commercial devices depending on oxide thickness and photon energy (*7*, *17*). Larger sensitivities are achieved when a positive bias is applied to the gate electrode, as the electric field improves exciton dissociation (*18*–*20*). RADFET dosimeters have been used to monitor radiation doses in radiotherapy (*6*, *7*) or space missions (*17*). Incorporation of floating gate RADFET (*21*, *22*) in monolithic CMOS-integrated circuits has been achieved, and the integrated chip was used in miniaturized, low-power dosimeters with wireless data transmission (*23*, *24*).

To achieve improved performance of RADFET dosimeters, a change in materials is required as the sensitivity is currently limited by the low stopping power of silicon oxide, and their integration into dense arrays on flexible plastic foil is incompatible with silicon CMOS technology. Amorphous semiconducting oxides (*25*) such as indium-gallium-zinc oxide (IGZO) and FETs made thereof have experienced a rapid development in recent years and represent a mature technology platform used in large-area electronics (*26*–*28*). They combine highly stable electronic performance, with mobilities exceeding 10 cm^2/Vs, with low-temperature processing on large-area substrates by sputtering- or solution-based processing to realize flexible FET arrays used, for example, as analog amplifiers (*29*) or as active matrices to address luminescent or sensor pixels. For radiation sensors, amorphous semiconducting oxides have further advantages as they exhibit excellent radiation hardness (*30*), and their facile processing allows combination with a wide range of dielectrics (*31*), thus allowing for optimization of ionization space charge buildup.

[1]Department of Physics and Astronomy, University of Bologna, Viale Berti Pichat 6/2, 40127 Bologna, Italy. [2]CENIMAT/I3N and CEMOP-UNINOVA, Departamento de Ciência dos Materiais, Faculdade de Ciências e Tecnologia, Universidade Nova de Lisboa, Campus de Caparica, 2829-516 Caparica, Portugal. [3]Tagsys RFID, 785 Voie Antiope, 13600 La Ciotat, France.
*Corresponding author. Email: tobias.cramer@unibo.it

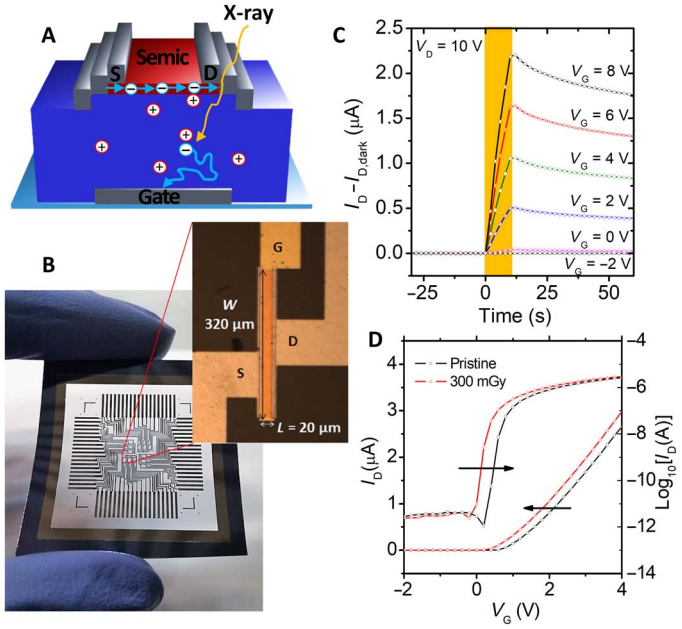

Fig. 1. Oxide thin-film transistors as direct detectors for x-ray radiation. (**A**) Scheme showing the transistor structure and the generation of trapped positive charge in the dielectric as a consequence of x-ray absorption. Negative carriers accumulating in the channel counterbalance the trapped positive charge. (**B**) Photograph showing a flexible matrix of IGZO-based transistors fabricated on a PEN foil. The inset shows a micrograph of a single transistor pixel. (**C**) Variation in oxide transistor drain current as a function of time, before, during (yellow background, 35-keV Mo tube, 300-mGy total dose), and after a 10-s x-ray exposure at varying gate voltages. (**D**) Transistor transfer curves acquired before and after exposure to 300-mGy radiation dose. Semic, semiconductor.

Here, we introduce the radiation-sensitive oxide semiconductor FET (ROXFET) that uses IGZO as a semiconductor and a multilayer dielectric containing tantalum oxide to increase stopping power and dielectric permittivity and silicon oxide to exhibit low interfacial trap state density and low leakage. We demonstrate that the multilayer exhibits positive space charge buildup under ionizing radiation in analogy to RADFETs, but with an order-of-magnitude increased sensitivity when operated in passive mode, that is, without applying an electric field to facilitate exciton separation. The optimized ROXFET sensor can easily be patterned into arrays on flexible plastic substrates, and we show the integration with low-cost CMOS radiofrequency identification (RFID) tags to yield a passive radiofrequency dosimeter tag operating in real time.

RESULTS

Radiation-sensitive oxide FETs

A flexible ROXFET sensor array on polyethylene naphthalate (PEN) foil is shown in Fig. 1B. The transistors contain an IGZO semiconducting channel of dimensions L = 20 μm and W = 320 μm contacted by a Mo source and a drain electrode. The optimized multilayer dielectric contains silicon oxide and tantalum oxide deposited by a co-sputtering process to combine low leakage with high x-ray sensitivity due to its increased high-Z atomic content. We used a patterned Mo gate electrode to accumulate carriers by field effect in the channel while it keeps a low parasitic capacitance to source and drain electrodes (C_p < 4 pF). In this configuration, depending on dielectric thickness, we obtain thin-film transistor (TFT) mobilities in the range of 10 to 22 cm^2/Vs, a steep subthreshold swing (0.16 to 0.35 V/decade), low leakage currents (<1 pA), and stable operation up to frequencies of 1 MHz (see fig. S1 and table S1). Figure 1C shows the x-ray photocurrent response of the transistor when subjected to a 10-s x-ray exposure (35-keV Mo tube, 29 mGy/s starting at t = 0 s). At positive gate potential, that is, in accumulation mode for the n-type semiconducting material, the channel current increases rapidly during the exposure. After the 10-s exposure, the current decays on a much slower time scale, indicating a large photoconductive gain (*9*). Shifting the gate potential to negative potentials, the photo response reduces in amplitude until no significant signal is observed when operated in a depletion mode (ΔI_D < 100 pA at V_G = −2 V). The observed transients are fully explained by a variation in threshold voltage due to x-ray exposure in analogy to the process known for silicon CMOS–based transistors. Figure 1D shows transfer characteristics obtained before and directly after exposure to 300 mGy of radiation. One notices a shift of the transfer curve to negative gate voltages, in agreement with the accumulation of positive ionization charge in the dielectric. No other TFT parameter such as subthreshold slope or mobility is affected, simultaneously confirming the radiation sensitivity of the transistor structure and the radiation hardness of oxide semiconductor transport properties (*30*).

To investigate the ROXFET response to x-ray radiation in detail, we expose the transistors to different x-ray radiation doses with all contacts connected to ground. We measure the transfer characteristics in a short measurement time interval of 6 ms (see fig. S2 for details) every 2 s. As depicted in Fig. 2A, each exposure leads to a characteristic shift in threshold voltage toward negative values. The inset shows that the shift in threshold voltage scales linearly with the exposure dose, thus allowing to define a sensitivity S in units of volts per gray. Here, the sensitivity value amounts to S = 3.4 ± 0.2 V/Gy, outperforming typical CMOS RADFET devices by about an order of magnitude.

When observing the ROXFET response on a longer time scale, one notices (Fig. 2B) that the threshold voltage returns to the initial value after exposure, thus indicating the annealing of positive ionization charge in the dielectric. The dynamics of the annealing process cannot be described by a single exponential but has contributions at different time scales resulting in a stretched exponential behavior. The dynamics is independent on dose, and, after normalization, all time traces superimpose on a universal curve, as shown in Fig. 2C. Quantitatively, the behavior is described by a stretched exponential using a time constant of τ = 17.9 min and an exponent of γ = 0.67. Stretched exponential behavior results from processes that follow a distribution of time constants, characteristic for transport in amorphous, disordered energy landscapes (*32*, *33*). Here, we attribute the behavior to trap states in the dielectric that are distributed in their characteristic energy and therefore keep the ionization charges captured for different characteristic time scales. In comparison to silicon oxide–based RADFET sensors, the annealing happens on faster time scales, and corrections have to be included when the sensor is used as an integrative dosimeter over long time scales. We find that the trap annealing time can be further shortened by increasing temperature or by applying electric fields across the dielectric (fig. S4). In this way, it is possible to easily reset the dosimeter to its initial state and to reuse the device (*34*).

The dielectric of the proposed ROXFET plays a crucial role in obtaining high x-ray sensitivity and a high signal-to-noise ratio for dosimeter applications. In particular, it has to combine low leakage and high permittivity with high x-ray cross section and high quantum

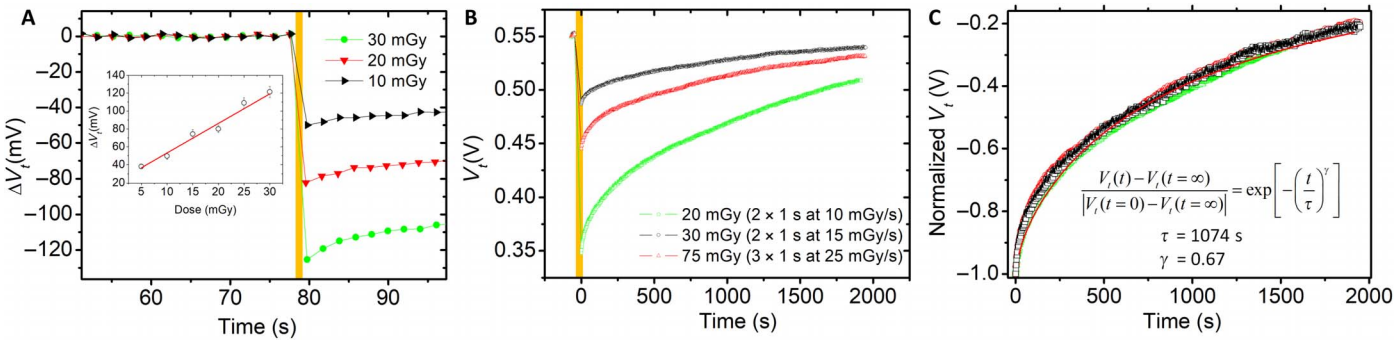

Fig. 2. Dynamics of ionization charge formation and recombination. (**A**) Threshold voltage shift of oxide transistor due to 1-s x-ray exposures of varying dose; inset shows the threshold voltage shift scales linearly with total exposure dose. (**B**) Threshold voltage as a function of time after x-ray exposure: Recombination processes lead to the annealing of trapped charges in the dielectric on a slow time scale. (**C**) Normalized threshold voltage shift for different exposure doses: The threshold recovers its initial value following a universal stretched exponential.

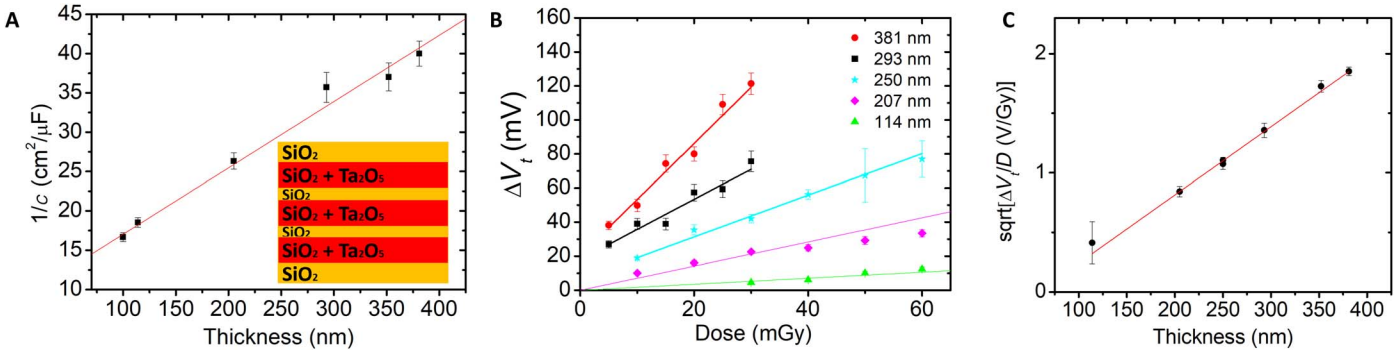

Fig. 3. Dependence of oxide-TFT detector on dielectric thickness. (**A**) Scaling of capacitance with dielectric thickness. The inset shows the multilayer structure of the dielectric. (**B**) Threshold voltage shift as a function of total dose for oxide transistors with different dielectric layers. (**C**) X-ray sensitivity, defined as the threshold voltage shift per dose, as a function of dielectric thickness. The line represents a quadratic fit according to the model described in the text.

efficiency. We developed a staked multilayer structure, as depicted in Fig. 3A, that uses alternating layers of sputtered SiO_2 and co-sputtered layers of Ta_2O_5 and SiO_2. The high content of high-Z tantalum atoms leads to 50 times shorter photon mean-free path than in pure SiO_2 dielectrics at the assessed x-ray energies that are beyond the tantalum x-ray absorption L-edge (see fig. S3). Layers of pure SiO_2 are incorporated to reduce the leakage current below 1 pA and to minimize the amount of interfacial trap states at the interface with the IGZO oxide semiconductor (*35*). Here, we observe steep subthreshold behavior with subthreshold slopes as low as 0.16 V/decade, revealing interfacial trap state densities $<10^{12}$ cm^{-2} eV^{-1}. Ta_2O_5 offers further advantages because of its properties as a high-κ dielectric (*36*). Figure 3A shows how the capacitance scales with the dielectric layer thickness. As expected, we observe a reciprocal relation, where the intercept is related to the interfacial layer of silicon oxide. The data fit well to a multilayer structure with alternating layers (*36*), yielding an effective permittivity of $\varepsilon_M = 13.4$. Because of this increased permittivity, we achieve specific capacitances of 25 nF/cm^2 in the TFTs with the thickest dielectric (382 nm), assuring a steep subthreshold slope and low-voltage operation. Next, we evaluate the impact of the multilayer dielectric thickness on x-ray sensitivity. Figure 3B shows the threshold voltage shifts obtained at different x-ray doses for transistors with varying dielectric thickness. For each tested device, a linear relation is obtained, and the resulting slope is reported in Fig. 3C as x-ray sensitivity as a function of layer thickness.

The quantitative description of the sensitivity as a function of multilayer dielectric layer thickness d (Fig. 3C) allows us to assess relevant parameters for the conversion of photons into ionization charge in these materials. Here, the increase of sensitivity follows a quadratic dependency, similar to what happens in classical RADFET dosimeters, due to the fact that the threshold voltage shift depends on the amount of accumulated charge density in the dielectric (σ) and on the specific dielectric capacitance (c): $\Delta V_{th} = \sigma/c$, where σ and $1/c$ increase with layer thickness (d) (*37*). The finding that the quadratic relation is also followed for larger thicknesses indicates that the characteristic traveling time of excited electrons out of the dielectric is much faster than electron hole recombination processes (*37*). Using only parameters related to material properties of the dielectric, the sensitivity can be described as (see Supplementary Information)

$$\frac{\Delta V_t}{\Delta D} = \frac{Q_I e}{2 c_{m,air} \varepsilon_M \varepsilon_0 \lambda W_{e\text{-}h}} d^2 \quad (1)$$

where e is the unit charge, $c_{m,air}$ is the mass attenuation coefficient of air for the unit conversion of the dose rate expressed in air kerma, ε_M is the permittivity of the multilayer as evaluated above, λ is the x-ray mean-free path, $W_{e\text{-}h}$ is the electron-hole pair creation energy, and Q_I is the efficiency of the conversion of absorbed photonic energy into trapped

charge carriers. We set the Mo-K_α line (17.5 keV) as the relevant photon energy to obtain values for $c_{m,air}$ and λ. Using $W_{e\text{-}h}$ = 12.9 eV that is three times the bandgap reported for Ta_2O_5 (*38*), we obtain Q_I = 16% from the linear fit of the sensitivity data (Fig. 3C).

Passive radiofrequency x-ray dosimeter tag

The here-proposed optimized multilayer dielectric endows the ROXFET with an increased x-ray sensitivity, a high-frequency operation, and a steep subthreshold behavior. The combination of these properties allow us to directly combine a ROXFET-based dosimeter with a passive RFID chip to achieve a low-cost x-ray dosimeter tag, as shown in Fig. 4. The main purpose of such an x-ray tag is to provide information upon wireless interrogation if the integrated received radiation dose has overcome a certain programmable threshold. Upon the RFID reader command, the integrated RFID tag probes the channel impedance *Z* of the ROXFET that has changed its value in case of radiation exposure (Fig. 4D). A simple version of such a functionality is implemented in commercial RFID chips as a tamper alarm, and switching occurs if the measured impedance varies from below 2 megohms to above 20 megohms. X-ray exposure can actually induce such an order-of-magnitude variation in the ROXFET channel impedance because of the resulting charging of the dielectric and the threshold voltage shift that is large enough to turn the transistor from an off state to an on state. This switch in state is then communicated by the RFID chip in the digital information that is contained in the reflected RF signal. An optical photography in Fig. 4B shows how we connect the commercial RFID chip to the antenna and to a single pixel of the ROXFET array in a prototype device realized on flexible PEN foil. To set the channel of the unexposed device fully in the off state, we connect a capacitance between gate and source and charge it with a programming voltage V_C. Figure 4C illustrates the impact of V_C on channel impedance at the relevant probing frequency of the RFID tag (1 kHz). At V_C values below 0 V, the channel is in the off state and the impedance is >20 megohms, so the RFID tag remains in the off state. We note that the impedance of the ROXFET in the off state results mostly from the parasitic capacitance due to overlap between gate and source/drain electrodes rather than dc-off current. Moving to positive V_C values, charge carriers accumulate in the channel, the transistor turns on, and the impedance drops. Within an interval of 0.6 V, the channel impedance lowers an order of magnitude down to <2 megohms, and the RFID chip changes its memory status. Figure 4D shows how x-ray exposure affects channel impedance. Three dosimeter tags are compared, after being initially charged with different V_C voltages to program different x-ray threshold doses. In the initial states, all dosimeters are in the high-impedance state, and the impedance remains high and constant also after the voltage source used to program V_C is removed. At t = 0, the devices are exposed to x-ray, and the impedances start to drop during exposure. The reduction in impedance continues until the x-ray exposure is stopped, as indicated by the arrows in the figure. After the exposure, we observe a slow recovery to the high-impedance state happening on time scales of several tens of seconds. Charging of the capacitance with the V_C voltage allowed us to program the x-ray threshold dose by controlling the impedance variation during x-ray exposure: Because of the V_C voltage, an electric field builds up across the multilayer dielectric of the ROXFET. Before ionization charges can induce carrier accumulation in the channel by field effect, they have to compensate the V_C field. Accordingly, we observe that more negative V_C voltages require longer exposure times to sufficiently decrease the channel impedance for RFID status switching. The inset shows the dependence of the critical dose needed to switch the RFID state as a function of V_C voltage. The graph demonstrates that the ROXFET-based, passive RFID dosimeter allows to detect programmable threshold doses in the range of hundreds of milligrays.

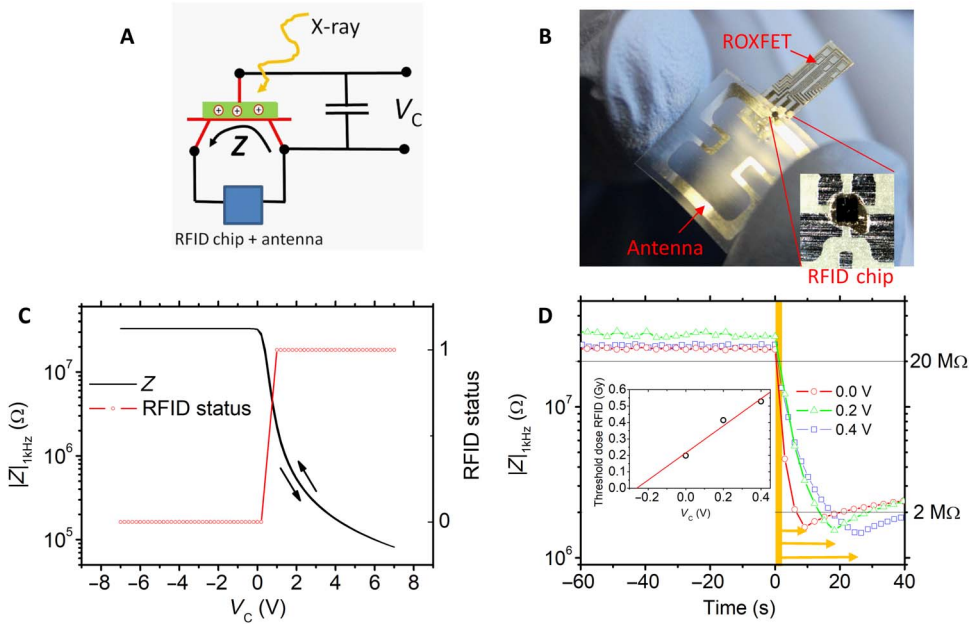

Fig. 4. Programmable passive RFID radiation sensor based on ROXFET. (**A**) Electrical circuit diagram showing how the radiation-sensitive oxide TFT is connected to the commercial passive RFID sensor and how the programming voltage V_C is applied. (**B**) Picture of flexible RFID x-ray sensor tag. (**C**) TFT channel impedance *Z* as a function of V_C. The RFID switches its status in a narrow interval close to the turn-on voltage of the transistor. (**D**) Channel impedance *Z* as a function of time for different RFID programming voltages V_C. At time = 0, the sensor was exposed to x-ray (30 mGy/s) for the indicated amount of time, leading to an order-of-magnitude decrease in *Z* and switching the RFID status. The inset shows the obtained threshold dose necessary to switch RFID status as a function of V_C.

DISCUSSION

The here-demonstrated integration of a microelectronic dosimeter with passive RFID technology for readout became possible because of the optimization of the ROXFET dielectric, that is, the crucial layer for x-ray–induced charge accumulation. The low-temperature sputtering process used in the fabrication of ROXFET allowed to introduce a multilayer dielectric that combines high-Z atomic content with high-κ properties, low leakage, and low interfacial trap density all on plastic, flexible substrates. Tantalum oxide is incorporated to reduce the x-ray attenuation length because of due to its high atomic number. As described in literature, tantalum oxide nanoparticles were previously used to increase radiopacity in dental fillings (*39*) or to improve x-ray absorption in organic direct x-ray detectors (*40*). Here, an order-of-magnitude reduction in attenuation length in the dielectric is achieved, translating in an order-of-magnitude increase in sensitivity with respect to literature values reported for silicon CMOS RADFETs (*7*, *17*). Tantalum oxide offers further the advantage of being a high-κ material well characterized and exploited in microelectronics (*36*). Because of the high-κ properties, ROXFETs with thick dielectric layers also show a steep subthreshold swing and low-voltage operation. Further, we suggest that the high-κ properties are relevant to support charge-carrier separation and positive-charge trapping after x-ray–induced exciton formation in the dielectric. In this way, a significant internal quantum efficiency of 16% for ionization charge buildup in the ROXFET dielectric is also observed in the absence of external electric fields. Drawbacks of tantalum oxide deposited by sputtering are well known and include a high interfacial trap density and leakage current (*41*). We successfully migrated these drawbacks by implementing a multilayer architecture in which the interfacial layers are sealed by sputtered silicon oxide layers. This approach has already been demonstrated to yield optimized performance in flexible oxide semiconductor transistors (*35*). All our processing steps are performed at low temperatures, compatible with polymeric substrates such as PEN, and flexible large-area dosimeter arrays that can provide spatially resolved information are realized (*42*). The developed oxide materials allow direct patterning of transistors on the plastic foil, achieving much higher integration densities and sensing performance (Fig. 1B) than the currently proposed state-of-the-art dosimeters for radiation therapy, fabricated by gluing small CMOS-RADFET pixels onto a flexible foil (*7*).

The high performance of the oxide FETs in terms of mobility, bandwidth, low-voltage operation, and high impedance is crucial to achieve readout with passive RFID technology that has to use ultralow-power probing signals. Here, using a commercial passive RFID chip, a RFID sensor tag is realized that measures whether an excess of an x-ray threshold dose occurs and communicates this information in digital form in the reflected RF signal together with its ID code to the receiver. We note that this digital transmission offers several advantages for sensing with respect to standard RF tags in which the sensing event affects the Q-factor of the antenna. The operating range for the wireless detector is demonstrated in the range of milligray (from a few to thousands) that is a relevant range for many applications in radiotherapy. An extension into the microgray range of operation is easily feasible for ROXFET-based detectors when using more specific readout electronics. The programming of the threshold dose of the RF dosimeter can be done by charging an external capacitance (Fig. 4A). Because of the low dielectric leakage of the ROXFET, such a voltage is maintained over long time scales ($\tau > 10^{13}$ ohms $\times 10^{-6}$ F $= 10^{7}$ s). Wireless, integrated dosimeters have been reported in the past (*23*, *24*); however, the direct integration of a passive real-time radiation sensor into a flexible, passive RFID tag with the here-reported performance is, to our knowledge, unprecedented and opens interesting possibilities for a range of novel applications. As the cost of such a tag is extremely low, one could imagine covering whole large areas with multiple sensor tags and remotely probing their status to assess x-ray exposure doses in radiation-intensive environments. As the tag provides the dose information in digital form together with a unique digital identifier, very dense positioning of sensor tags does not create problems, and doses can be attributed to unique sensor positions. For example, such a situation is relevant for radiotherapy when doses in the milligray range have to be delivered with high spatial resolution to treat tumors. The developed tag could be used to monitor in real time when the planned dose has been delivered and test also whether the spatial alignment of the beam has to be corrected, thereby improving treatment efficiency and patient security.

In conclusion, this work introduces oxide-based FETs as novel microelectronic x-ray dosimeters. The introduction of high-Z and high-κ materials into the amorphous layer stack of the transistor allowed to achieve x-ray sensitivities of up to 3.4 V/Gy, outperforming commercial silicon-based CMOS x-ray dosimeters by an order of magnitude in passive-mode operation. The radiation-sensitive transistors are fabricated on flexible foil, and their processing is compatible with large-area substrates. The low-voltage and high-frequency operation of the transistor enables readout of the dosimeter with passive CMOS-based RFID chips. The possibility to create a network of dispersed passive RF dosimeter tags or dosimeter arrays on flexible foils paves the way toward novel, spatially resolved x-ray dosimetry systems with application in radiotherapy, radioprotection, industrial applications, and space missions.

MATERIALS AND METHODS

Oxide TFTs with staggered bottom-gate, top-contact structure (see Fig. 1B) were fabricated entirely by RF magnetron sputtering without intentional substrate heating during deposition. The devices were fabricated on Corning Eagle glass or PEN substrates. A Mo gate electrode (60 nm thick) deposition was followed by a multicomponent and multilayer dielectric comprising seven layers of alternating SiO_2 and Ta_2O_5 + SiO_2 films (*43*). The total thickness of the dielectric was varied between 110 and 380 nm, but the ratio of total Ta_2O_5 + SiO_2 to SiO_2 layer thickness was kept constant at a value of $d_{Ta}/d_{Si} = 3.5$. The multilayer structure was obtained by co-sputtering from a SiO_2 target (at 1 nm/min) and a Ta_2O_5 target (at 3.4 nm/min). A 40-nm-thick IGZO semiconductor was then deposited from a multicomponent ceramic target with 2:1:1 (atomic In/Ga/Zn ratio) composition. Finally, 60-nm-thick Mo was sputtered for source and drain electrodes. The semiconductor and the source and drain electrodes were patterned by lift-off, while the gate and the dielectric were patterned by reactive ion etching in SF6 atmosphere. Final devices were annealed on a hot plate for 1 hour at 180°C. Width-to-length ratio (W/L) of the analyzed devices was 320/20 (μm/μm).

X-ray radiation was generated by a molybdenum tube, which was operated at a voltage of 35 kV and filament currents of 5 to 30 mA. The sample was positioned at 32 cm from the opening shutter of the tube. The resulting dose rate at the sample position was determined to be 5 to 29.9 mGy s^{-1} air kerma using a PMX-III dosimeter.

Oxide transistors were characterized with a Keysight B2912 measurement unit. During x-ray exposure, the three terminals of the TFTs were kept at ground potential. Transfer characteristics were acquired

every 2 s in a time interval of 6 ms. Transistor parameters were obtained by fitting the transfer characteristics to the standard metal oxide semiconductor FET model in the saturation regime $I_D = \frac{1}{2} \cdot \frac{W}{L} \cdot \mu \cdot C \cdot (V_G - V_t)^2$. Impedance measurements were performed with a Metrohm PGSTAT204. For RFID experiments, a 1-μF capacitance was connected between the source and gate electrodes. The RFID tag chip NXP SL3S1203_1213 fixed on a PEN foil with Al contacts and an antenna was obtained from Tagsys. The TFT source and drain electrodes were connected to the V_{DD} and V_{OUT} pin of the chip with silver paste. An Impinj R420 RFID reader operating at the European Industrial Scientific and Medical 868-MHz band was used to probe the tamper alarm flag of the RFID chip during x-ray exposure experiments or as a function of V_C.

SUPPLEMENTARY MATERIALS

Supplementary material for this article is available at http://advances.sciencemag.org/cgi/content/full/4/6/eaat1825/DC1

Supplementary Information

fig. S1. Fast transistor operation and switching: Gate capacitance C_G as a function of gate voltage V_{GS} for different frequencies.

fig. S2. Fast transfer characteristic acquisition.

fig. S3. Calculated attenuation length spectra for silicon oxide, tantalum oxide, and the multilayer dielectric based on National Institute of Standards and Technology database.

fig. S4. Accelerated recovery of ROXFET due to application of positive gate voltage.

table S1. Properties of a set of IGZO transistors with W = 320 μm and L = 20 μm and varying multilayer dielectric thickness.

REFERENCES AND NOTES

1. B. Camanzi, A. G. Holmes-Siedle, The race for new radiation monitors. *Nat. Mater.* **7**, 343–345 (2008).
2. A. G. Holmes-Siedle, L. Adams, S. Marsden, B. Pauly, Calibration and flight testing of a low-field pMOS dosimeter. *IEEE Trans. Nucl. Sci.* **32**, 4425–4429 (1985).
3. W. P. M. Mayles, R. Lake, A. McKenzie, E. M. Macaulay, H. M. Morgan, T. J. Jordan, S. K. Powley, *Physics Aspects of Quality Control in Radiotherapy* (IPEM, 1999).
4. I. Mandic, V. Cindro, A. Gorisek, G. Kramberger, M. Mikuz, Online integrating radiation monitoring system for the ATLAS detector at the large hadron collider. *IEEE Trans. Nucl. Sci.* **54**, 1143–1150 (2007).
5. J. Seco, B. Clasie, M. Partridge, Review on the characteristics of radiation detectors for dosimetry and imaging. *Phys. Med. Biol.* **59**, R303–R347 (2014).
6. W. L. Jong, N. M. Ung, J. H. D. Wong, K. H. Ngb, W. Z. Wan Ishaka, R. Abdul Malik, V. C. E. Phua, D. L. Cutajar, P. E. Metcalfe, A. B. Rosenfeld, G. F. Ho, In vivo skin dose measurement using MO*Skin* detectors in tangential breast radiotherapy. *Phys. Med.* **32**, 1466–1474 (2016).
7. R. A. Price, C. Benson, M. J. Joyce, K. Rodgers, Development of a RadFET linear array for intracavitary in vivo dosimetry during external beam radiotherapy and brachytherapy. *IEEE Trans. Nucl. Sci.* **51**, 1420–1426 (2004).
8. Y. C. Kim, K. H. Kim, D.-Y. Son, D.-N. Jeong, J.-Y. Seo, Y. S. Choi, I. T. Han, S. Y. Lee, N.-G. Park, Printable organometallic perovskite enables large-area, low-dose X-ray imaging. *Nature* **550**, 87–91 (2017).
9. L. Basiricò, A. Ciavatti, T. Cramer, P. Cosseddu, A. Bonfiglio, B. Fraboni, Direct X-ray photoconversion in flexible organic thin film devices operated below 1 V. *Nat. Commun.* **7**, 13063 (2016).
10. G. F. Knoll, *Radiation Detection and Measurement* (John Wiley & Sons, ed. 4, 2010).
11. A. G. Holmes-Siedle, The space charge dosimeter: General principles of a new method of radiation detection. *Nucl. Instrum. Methods* **121**, 169 (1974).
12. R. C. Hughes, W. R. Dawes Jr., W. J. Meyer, S. W. Yoon, Dual dielectric silicon metal-oxide-semiconductor field-effect transistors as radiation sensors. *J. Appl. Phys.* **65**, 1972 (1989).
13. G. Sarrabayrouse, V. Polischuk, MOS ionizing radiation dosimeters: From low to high dose measurement. *Radiat. Phys. Chem.* **61**, 511–513 (2001).
14. T. R. Oldham, F. B. McLean, Total ionizing dose effects in MOS oxides and devices. *IEEE Trans. Nucl. Sci.* **50**, 483–499 (2003).
15. T. P. Ma, P. V. Dressendorfer, *Ionizing Radiation Effects in MOS Devices and Circuits* (John Wiley & Sons, 1989).
16. C. R. Edwards, S. Green, J. E. Palethorpe, P. J. Mountford, The response of a MOSFET, p-type semiconductor and LiF TLD to quasi-monoenergetic x-rays. *Phys. Med. Biol.* **42**, 2383–2391 (1997).
17. A. G. Holmes-Siedle, J. O. Goldsten, R. H. Maurer, P. N. Peplowski, RADFET dosimeters in the belt: The Van Allen Probes on day 365, 14th European Conference on Radiation and Its Effects on Components and Systems (RADECS 2013), Oxford, UK, 23 to 27 September 2013.
18. G. Sarrabayrouse, S. Siskos, Low dose measurement with thick gate oxide MOSFETs. *Radiat. Phys. Chem.* **81**, 339–344 (2012).
19. G. S. Ristić, S. Golubović, M. M. Pejović, Sensitivity and fading of pMOS dosimeters with thick gate oxide. *Sens. Actuators A Phys.* **51**, 153–158 (1996).
20. A. Holmes-Siedle, L. Adams, G. Ensell, MOS dosimeters—Improvement of responsivity. *IEEE Trans. Nucl. Sci.* 65–69 (1986).
21. M. N. Martin, D. R. Roth, A. Garrison-Darrin, P. J. McNulty, A. G. Andreou, FGMOS dosimetry: Design and implementation. *IEEE Trans. Nucl. Sci.* **48**, 2050–2055 (2001).
22. N. G. Tarr, G. F. Mackay, K. R. Shortt, I. Thomson, A floating gate MOSFET dosimeter requiring no external bias supply. *IEEE Trans. Nucl. Sci.* **45**, 1470–1474 (1998).
23. M. Arsalan, A. Shamim, M. Shams, N. G. Tarr, L. Roy, Ultra low power CMOS-based sensor for on-body radiation dose measurements. *IEEE J. Emerg. Sel. Top. Circuits Syst.* **2**, 34–41 (2012).
24. F. Fuschino, A. Gabrielli, G. Baldazzi, R. Campana, S. Valentinetti, M. Crepaldi, D. Demarchi, E. G. Villani, A wireless transmission low-power radiation sensor for in vivo dosimetry. *J. Instrum.* **9**, C02016 (2014).
25. M. Lorenz, M. S. R. Rao, T. Venkatesan, E. Fortunato, P. Barquinha, R. Branquinho, D. Salgueiro, R. Martins, E. Carlos, A. Liu, F. K. Shan, M. Grundmann, H. Boschker, J. Mukherjee, M. Priyadarshini, N. DasGupta, D. J. Rogers, F. H. Teherani, E. V. Sandana, P. Bove, K. Rietwyk, A. Zaban, A. Veziridis, A. Weidenkaff, M. Muralidhar, M. Murakami, S. Abel, J. Fompeyrine, J. Zuniga-Perez, R. Ramesh, N. A. Spaldin, S. Ostanin, V. Borisov, I. Mertig, V. Lazenka, G. Srinivasan, W. Prellier, M. Uchida, M. Kawasaki, R. Pentcheva, P. Gegenwart, F. M. Granozio, J. Fontcuberta, N. Pryds, The 2016 oxide electronic materials and oxide interfaces roadmap. *J. Phys. D Appl. Phys.* **49**, 433001 (2016).
26. T. Kamiya, H. Hosono, Materials characteristics and applications of transparent amorphous oxide semiconductors. *NPG Asia Mater.* **2**, 15–22 (2010).
27. E. Fortunato, P. Barquinha, R. Martins, Oxide semiconductor thin-film transistors: A review of recent advances. *Adv. Mater.* **24**, 2945–2986 (2012).
28. K. M. Niang, P. M. C. Barquinha, R. F. P. Martins, B. Cobb, M. J. Powell, A. J. Flewitt, A thermalization energy analysis of the threshold voltage shift in amorphous indium gallium zinc oxide thin film transistors under positive gate bias stress. *Appl. Phys. Lett.* **108**, 093505 (2016).
29. P. G. Bahubalindruni, B. Silva, V. G. Tavares, P. Barquinha, N. Cardoso, P. G. de Oliveira, R. Martins, E. Fortunato, Analog circuits with high-gain topologies using a-GIZO TFTs on glass. *J. Disp. Technol.* **11**, 547–553 (2015).
30. T. Cramer, A. Sacchetti, M. T. Lobato, P. Barquinha, V. Fischer, M. Benwadih, J. Bablet, E. Fortunato, R. Martins, B. Fraboni, Radiation-tolerant flexible large-area electronics based on oxide semiconductors. *Adv. Electron. Mater.* **2**, 1500489 (2016).
31. R. F. P. Martins, A. Ahnood, N. Correia, L. M. N. P. Pereira, R. Barros, P. M. C. B. Barquinha, R. Costa, I. M. M. Ferreira, A. Nathan, E. E. M. C. Fortunato, Recyclable, flexible low-power oxide electronics. *Adv. Funct. Mater.* **23**, 2153–2161 (2013).
32. B. Sturman, E. Podivilov, M. Gorkunov, Origin of stretched exponential relaxation for hopping-transport models. *Phys. Rev. Lett.* **91**, 176602 (2003).
33. J. Luo, A. U. Adler, T. O. Mason, D. B. Buchholz, R. P. H. Chang, M. Grayson, Transient photoresponse in amorphous In-Ga-Zn-O thin films under stretched exponential analysis. *J. Appl. Phys.* **113**, 153709 (2013).
34. J. Lipovetzky, E. G. Redin, A. Faigón, Electrically erasable metal–oxide–semiconductor dosimeters. *IEEE Trans. Nucl. Sci.* **54**, 1244–1250 (2007).
35. J. Liu, D. B. Buchholz, J. W. Hennek, R. P. H. Chang, A. Facchetti, T. J. Marks, All-amorphous-oxide transparent, flexible thin-film transistors. Efficacy of bilayer gate dielectrics. *J. Am. Chem. Soc.* **132**, 11934–11942 (2010).
36. C. Chaneliere, J.-L. Autran, R. A. B. Devine, B. Balland, Tantalum pentoxide (Ta_2O_5) thin films for advanced dielectric applications. *Mater. Sci. Eng. R* **22**, 269–322 (1998).
37. R. C. Hughes, Theory of response of radiation sensing field-effect transistors in zero-bias operation. *J. Appl. Phys.* **60**, 1216–1217 (1986).
38. J. Han, Q. Zhang, W. Fan, G. Feng, Y. Li, A. Wei, R. Hu, Q. Gu, The characteristics of Ta_2O_5 films deposited by radio frequency pure oxygen ion assisted deposition (RFOIAD) technology. *J. Appl. Phys.* **121**, 065302 (2017).
39. H. Schulz, L. Mädler, S. E. Pratsinis, P. Burtscher, N. Moszner, Transparent nanocomposites of radiopaque, flame-made Ta_2O_5/SiO_2 particles in an acrylic matrix. *Adv. Funct. Mater.* **15**, 830–837 (2005).
40. C. A. Mills, H. Al-Otaibi, A. Intaniwet, M. Shkunov, S. Pani, J. L. Keddie, P. J. Sellin, Enhanced x-ray detection sensitivity in semiconducting polymer diodes containing metallic nanoparticles. *J. Phys. D Appl. Phys.* **46**, 275102 (2013).
41. R. M. Fleming, D. V. Lang, C. D. W. Jones, M. L. Steigerwald, D. W. Murphy, G. B. Alers, Y.-H. Wong, R. B. van Dover, J. R. Kwo, A. M. Sergent, Defect dominated charge transport in amorphous Ta_2O_5 thin films. *J. Appl. Phys.* **88**, 850–862 (2000).

42. G. I. Kaplan, A. B. Rosenfeld, B. J. Allen, J. T. Booth, M. G. Carolan, A. G. Holmes-Siedle, Improved spatial resolution by MOSFET dosimetry of an x-ray microbeam. *Med. Phys.* **27**, 239–244 (2000).
43. P. Barquinha, L. Pereira, G. S. Gonçalves, R. Martins, D. Kuščer, M. Kosec, E. Fortunato, Performance and stability of low temperature transparent thin-film transistors using amorphous multicomponent dielectrics. *J. Electrochem. Soc.* **156**, H824–H831 (2009).

Acknowledgments
Funding: This work was funded by the European Union (EU) seventh Framework Programme (FP7/2007–2013) under grant agreement no. 611070, "Integrated Flexible Photonic Sensors System (iFLEXIS)" and by the EU Horizon 2020 Programme (European Research Council) under grant agreement no. 716510, "Transparent and flexible electronics with embedded energy harvesting based on oxide nanowire devices (TREND)" projects. Further funding is acknowledged from FEDER funds through the COMPETE 2020 Programme and National Funds through the Portuguese Foundation for Science and Technology (FCT) under project no. UID/CTM/50025/2013. **Author contributions:** Oxide transistors where fabricated by A.S., C.F., and I.F. X-ray response of oxide transistors was characterized by I.F. and T.C. The RFID tag was designed and tested by F.D., C.L., and T.C. B.F., P.B., E.F., and R.M. supervised the research. All authors discussed the data and contributed to the manuscript writing. **Competing interests:** T.C., B.F., P.B., R.M., and E.F. are inventors on a international patent application related in part to this work (serial no. PCT/IT2017/000050, priority date: 14 November 2016). All other authors declare that they have no competing interests. **Data and materials availability:** All data needed to evaluate the conclusions in the paper are present in the paper and/or the Supplementary Materials. Additional data related to this paper may be requested from the authors.

Submitted 3 February 2018
Accepted 18 May 2018
Published 29 June 2018
10.1126/sciadv.aat1825

Citation: T. Cramer, I. Fratelli, P. Barquinha, A. Santa, C. Fernandes, F. D'Annunzio, C. Loussert, R. Martins, E. Fortunato, B. Fraboni, Passive radiofrequency x-ray dosimeter tag based on flexible radiation-sensitive oxide field-effect transistor. *Sci. Adv.* **4**, eaat1825 (2018).

ScienceAdvances

Passive radiofrequency x-ray dosimeter tag based on flexible radiation-sensitive oxide field-effect transistor

Tobias Cramer, Ilaria Fratelli, Pedro Barquinha, Ana Santa, Cristina Fernandes, Franck D'Annunzio, Christophe Loussert, Rodrigo Martins, Elvira Fortunato and Beatrice Fraboni

Sci Adv **4** (6), eaat1825.
DOI: 10.1126/sciadv.aat1825